Supporting Information for

Breaking the Symmetry of Sulfur Defect State via Atomic Substitution for Enhanced CO_2 Photoreduction

Yingxin Ma,[a]† Haolan Tao,[b]† Xuyun Guo,[c]† Peinuo Yang,[a] Dan Xing,[a] Valeria Nicolosi,[c] Yu Zhang,[d] Cheng Lian, [b]* and Bocheng Qiu [a]*.*

[a] Department of Chemistry, College of Sciences, Nanjing Agricultural University, Nanjing 210095, China.

[b] State Key Laboratory of Chemical Engineering, Shanghai Engineering Research Center of Hierarchical Nanomaterials, School of Chemistry and Molecular Engineering, East China University of Science and Technology, Shanghai, 200237 China.

[c] School of Chemistry, Centre for Research on Adaptive Nanostructures and Nanodevices (CRANN) and Advanced Materials Bio-Engineering Research Centre (AMBER), Trinity College Dublin, Dublin, D02PN40 Ireland.

[d] College of Energy and Power Engineering, Nanjing Institute of Technology, Nanjing 211167, China.

† These authors contributed equally to this work

***Corresponding Authors**

E-mail: bochengqiu@njau.edu.cn; liancheng@ecust.edu.cn; yu_zhang1225@163.com.

Materials and Methods

Chemicals

Stannic chloride pentahydrate ($SnCl_4 \cdot 5H_2O$, 99%), and sodium sulfate anhydrous (Na_2SO_4, 99%) were purchased from Shanghai Macklin Biochemical Technology Co., Ltd. L-cysteine (99%), copper chloride dihydrate ($CuCl_2 \cdot 2H_2O$, 99%), sodium dodecyl benzene sulfonate (SDBS, 99%) were purchased from Shanghai Aladdin Bio-Chem Technology Co., Ltd. Anhydrous ethanol (C_2H_5OH, 99.5%) and potassium bicarbonate ($KHCO_3$, 99%) were purchased from Sinopharm Chemical Reagent Co., Ltd. (Shanghai, China). All the chemicals were used without purification. Deionized (DI) water (18.25 MΩ cm) was used in all experiments.

Preparation of SnS_2-S_V

0.25 mmol $SnCl_4 \cdot 5H_2O$ and 2 mmol L-cysteine were dissolved into 30 mL deionized (DI) water. After stirring for 30 min, 0.6 mmol sodium dodecyl benzene sulfonate (SDBS) was added into the above solution. After stirring for another 30 min, the solution was transferred into a 50 mL autoclave and maintained at 160 ^oC for 12 h. After cooling down, the SnS_2-S_V sample was collected, washed with DI water and ethanol for several times, and finally freeze-dried for further uses.

Preparation of Cu-SnS_2-S_V

0.25 mmol $SnCl_4 \cdot 5H_2O$, 0.025 mmol $CuCl_2 \cdot 2H_2O$, and 2 mmol L-cysteine were dissolved into 30 mL deionized (DI) water. After stirring for 30 min, 0.6 mmol sodium dodecyl benzene sulfonate (SDBS) was added into the above solution. After stirring for another 30 min, the solution was transferred into a 50 mL autoclave and maintained at 160 ^oC for 12 h. After cooling down, the Cu-SnS_2-S_V sample was collected, washed with deionized water and ethanol for several times, and then freeze-dried for further uses. To confirm the optimal Cu doping level, the Cu-Sn-S_V catalyst with different Cu doping concentrations were prepared (1.25%, 2.5%, 5%, and 20%, which indicate the molar percentage of the Cu dopant to Sn).

Photocatalytic experiments

CO_2 photoreduction performance over the as-prepared catalysts was evaluated in an online sealed Pyrex photocatalysis system (Labsolar-6A, Beijing Perfectlight) under a simulated sunlight irradiation. 20 mg powder catalyst was dispersed into 10 mL water via an ultrasonic treatment, and the as-obtained dispersion was subsequently added in a 55 mm diameter Petri dish and dried at room temperature. The dish coated with the sample was placed in the sealed Pyrex photocatalysis system. Before illumination, pumping vacuum and purging with CO_2 (99.999%) were carried out alternately, and 0.8 atm CO_2 was eventually maintained in the reactor. 1 mL deionized water was then injected into the reactor, and the built-in fan was initiated for 30 min until the H_2O and CO_2 were evenly mixed. The evolved gas was analyzed by gas chromatograph (FULI INSTRUMENTS GC9790Plus) equipped with a thermal conductivity detector (TCD), flame ionization detector (FID), and a molecular sieve column with Ar as the carrier gas. The apparent quantum efficiencies (AQE) for CO evolution was calculated according to the following

equation: AQE= (numbers of the electrons taking part in CO evolution)/(numbers of the incident photons) x 100%

In-situ DRIFTS experiments

In-situ diffuse reflection infrared Fourier-transform spectroscopy were recorded on a Bruker IFS 66v Fourier-transform spectrometer equipped with a Harrick diffuse reflectance accessory at the Infrared Spectroscopy and Micro spectroscopy End station (BL01B) in NSRL in Hefei, China. The samples were directly sealed in a custom-fabricated infrared (IR) reaction chamber. CO_2 and H_2O were introduced into the reaction chamber by N_2 flow until equilibrium. With the equilibrium system before reaction as the background, IR signals were collected during the incident irradiation of a 300 W Xe lamp through the quartz glass window.

Material Characterizations

A RigakuD/MAX IIIA diffract meter with Cu Kα radiation (λ =1.5418 Å) was used to collect the X-ray diffraction (XRD) patterns of all the catalysts in the range 10-80° (2θ). The morphologies and HRTEM images of all samples were characterized using uncorrected FEI Titan with Schottky field emission S-FEG source operated at 300 kV. Electron energy-loss spectroscopy (EELS) mapping was carried out with Quantum Gatan Imaging Filter (GIF) detector with energy dispersion of 0.5 eV per channel. Aberration-corrected scanning transmission electron microscopy (AC-STEM) was performed on a Nion UltraSTEM 200 microscope equipped with a cold field emission gun and a quadrupole-octupole type probe corrector, Bruker Quantax EDS detector and Gatan Enfinium EELS detector. The microscope was operated at 200 kV with a 27 mrad convergence semi-angle. The collection semi-angle for MAADF was 46-200 mrad. Dual EELS mode with energy dispersion of 0.25 eV per channel and 40 mrad collection angle were set up for AC-STEM EELS. Atomic Force Microscopy (AFM) for thickness measurements was recorded on scanning probe microscope (Bruker Dimension Icon). XPS analysis was recorded on a Perkin-Elmer PHI 5000C ESCA system with Al Kα radiation (hν=1486.6 eV) with a spot size of 500 μm operated at 250 W. Ultraviolet photoelectron spectroscopy (UPS) was carried out on Thermo ScientificTM K-Alpha He I resonance line (hν=21.22 eV). Photocurrent response and measurements and electrochemical impedance spectroscopy were carried out on a standard three-electrode cell with a working electrode, a graphite rod as the counter electrode, and a saturated calomel electrode as the reference electrode in dark on a Corrtest electrochemical workstation (CS300MA). The working electrode was prepared via deposition of a sample film on a clean fluoride-tin oxide (FTO). The aqueous solution containing 0.5 M Na_2SO_4 purged with nitrogen gas was used as an electrolyte. Linear sweep voltammetry (LSV) curves were recorded in a CO_2-saturated $KHCO_3$ electrolyte at a scan rate of 5 mV s^{-1}. Time-resolved transient photoluminescence (PL) spectra were performed on Edinburgh FLS980 and fitted with a bi-exponential function fitting curves. Inductively coupled plasma-massspectrometry (ICP-MS, Agilent 7700x, USA) was utilized to determine the Cu doping levels. To trace the origin for CO evolution, $^{13}CO_2$ was used as feedstocks, and the evolved gaseous products were analyzed

by gas chromatography-mass spectrometer (GC-MS, Agilent 5975C Mass Selective Detector using triple-axis-detector in the electron impact ionization mode).

X-ray absorption spectroscopy (XAS) data analysis

The X-ray absorption fine structure spectra (Cu K-edge) were collected at BL14W1 beamline at the Shanghai Synchrotron Radiation Facility. The standard procedures were applied to process the acquired EXAFS data using the ATHENA module in the IFEFFIT software packages. The post-edge background was subtracted from the overall absorption and then normalized to the edge-jump step to obtain the k^3-weighted EXAFS spectra. A Hanning window was used to Fourier transform the k^3-weighted $\chi(k)$ data of Cu K-edge to real R space and separate the EXAFS contributions from different coordination shells. Using the ARTEMIS module of the IFEFFIT software packages, least-squares curve parameter fitting was applied to obtain the quantitative structural parameters around central atoms. All the curves are plotted without using phase correction.

Theoretical calculations

Density functional theory (DFT) calculations were carried out using the Vienna *ab initio* Simulation Package (VASP) with the projector augmented wave (PAW) method.[1-3] The Perdew-Burke-Ernzerhof (PBE) exchange-correlation functional was chosen.[4] For density of states (DOS) calculations, the standard Heyd-Scuseria-Ernzerh (HSE06) hybrid functional was employed to obtain reasonably accurate band gaps. The Brillouin zone was sampled with the Γ-centered 3×3×1 Monkhorst-Pack k-mesh. The cut-off energy for the plane-wave basis set was 450 eV. The convergence criterion for the electronic self-consistent iteration was set to be 10^{-5} eV. The force tolerance for structural relaxation was 0.01 eV·Å^{-1}. The vacuum thickness was set to 15 Å to ensure decoupling between neighboring slabs.

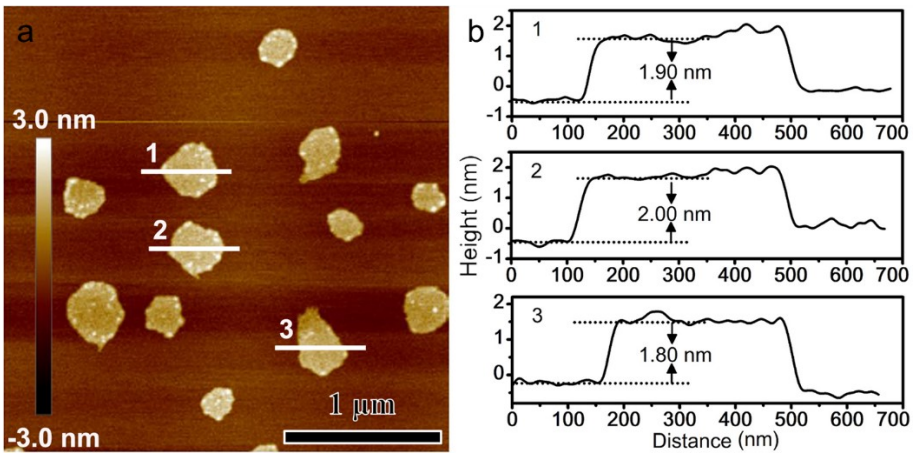

Fig. S1 (a) AFM image of Cu-SnS_2-S_V and (b) its corresponding height profiles.

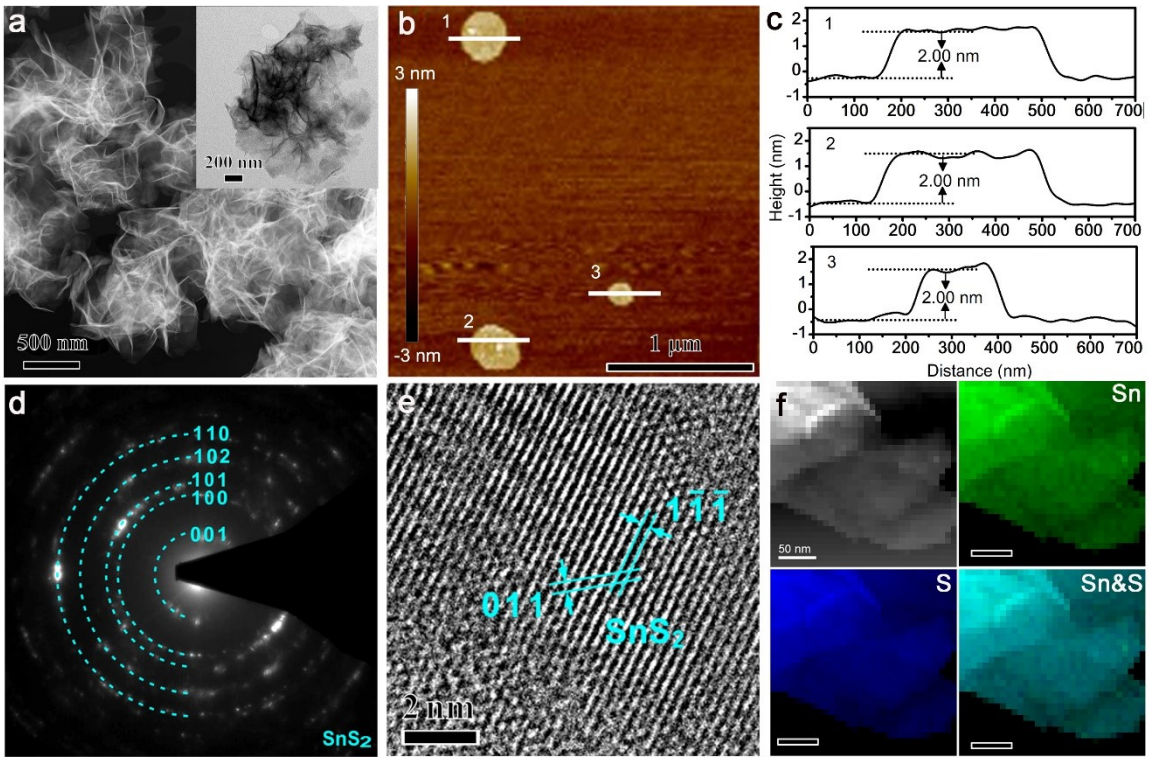

Fig. S2 (a) STEM image (the inset is the TEM image), (b) AFM image and (c) its corresponding height profiles, (d) SAED pattern, (e) HRTEM image, and (f) HAADF-STEM image and its corresponding EELS elemental mapping of SnS_2-S_V.

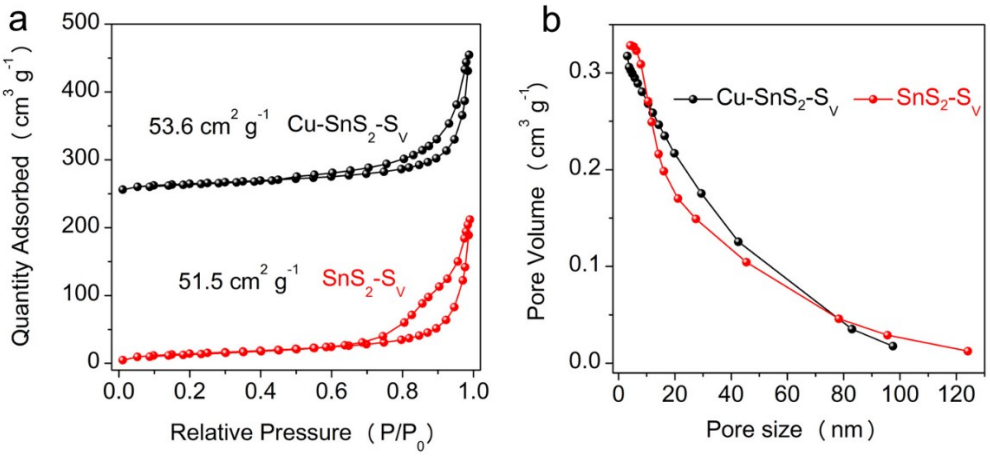

Fig. S3 (a) Nitrogen adsorption and (b) desorption curves of Cu-SnS_2-S_V and SnS_2-S_V and their pore size distributions.

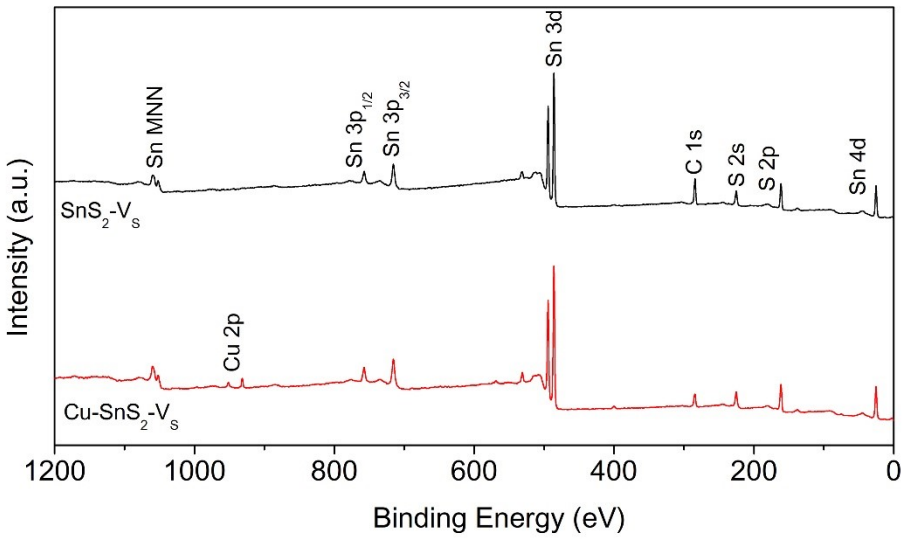

Fig. S4 XPS survey spectra of Cu-SnS_2-S_V and SnS_2-S_V.

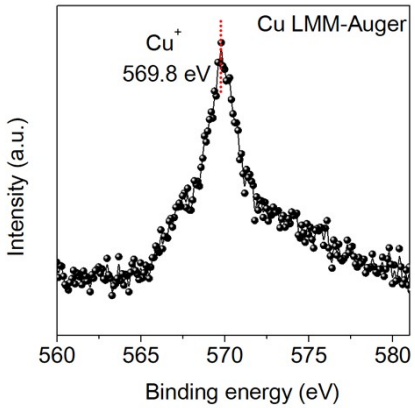

Fig. S5 The Cu LMM auger XPS spectrum of Cu-SnS_2-S_V. The Cu LMM Auger electron spectroscopy (AES) spectrum shows that the main peak locates at 569.8 eV, corresponding to Cu^+ species.[5]

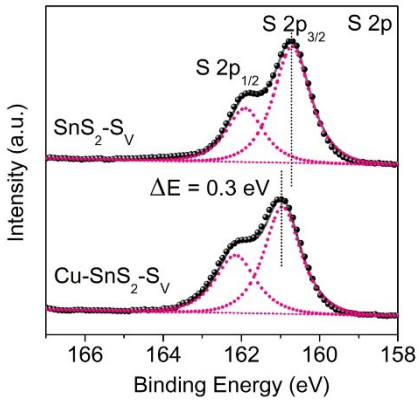

Fig. S6 S 2p XPS spectra of Cu-SnS_2-S_V and SnS_2-S_V.

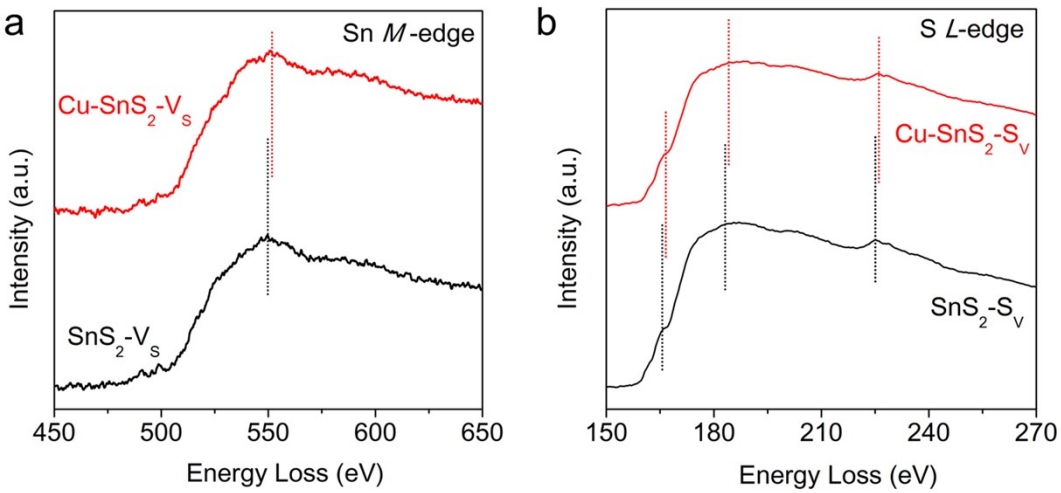

Fig. S7 EELS profiles for (A) Sn *M*-edge and (B) S *L*-edge spectra of Cu-SnS_2-S_V and SnS_2-S_V.

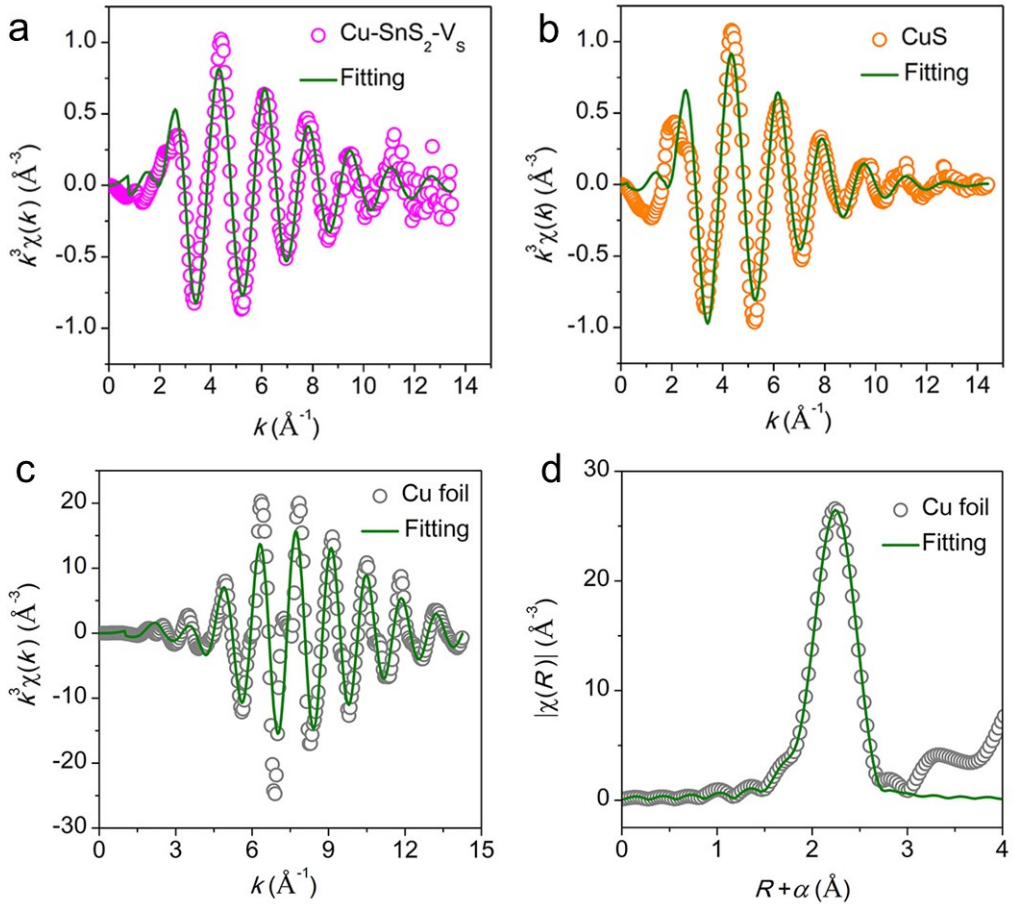

Fig. S8 Cu K-edge EXAFS and the fitting curves for Cu-SnS_2-S_V (a), CuS (b), and Cu foil (c, d). Fitting results are shown in k-space (a, b, and c), and in R-space (d). All the curves are plotted without using phase correction.

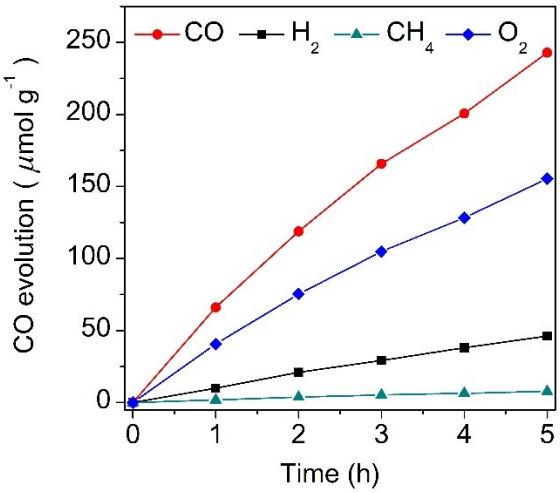

Fig. S9 CO, CH_4, H_2, and O_2 amounts detected in a 5-h run over Cu-SnS_2-S_V. The selectivity in hydrocarbon production is calculated based on the consumed electrons using the following equation: Selectivity (%) = $[2v(CO)]/[2v(CO) + 8v(CH_4) + 2v(H_2)] \times 100\%$, where $v(CO)$, $v(CH_4)$, and $v(H_2)$ indicate the formation rates for CO, CH_4, and H_2, respectively. The CO, CH_4, and H_2 selectivities over Cu-SnS_2-S_V were thus calculated to be 75.8%, 9.8%, and 14.4%, respectively.

The consumed electrons for CO, H_2, and CH_4 evolution over Cu-SnS_2-S_V (1 g) in 5 h are calculated to be approximately 642 μmol (243*2+46*2+8*8=642 μmol). The consumed holes for O_2 evolution over Cu-SnS_2-S_V (1 g) in 5 h are determined to be 620 μmol (155*4=620 μmol). The ratio of electron to hole is calculated to be 1.04.

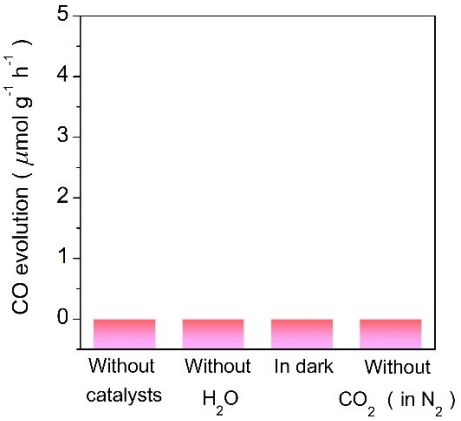

Fig. S10 CO production rate recorded under different reaction conditions.

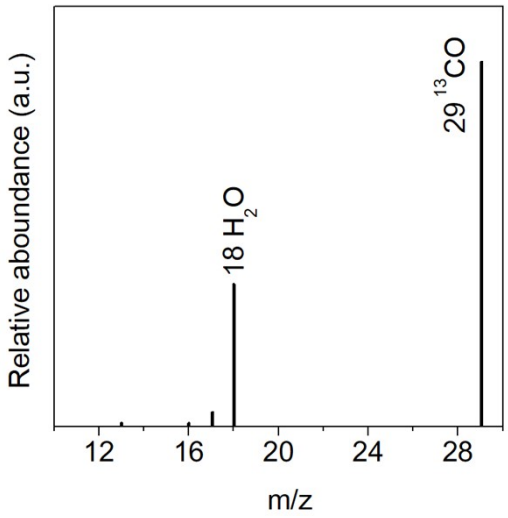

Fig. S11 GC-MS analysis for CO produced from $^{13}CO_2$ isotope experiment.

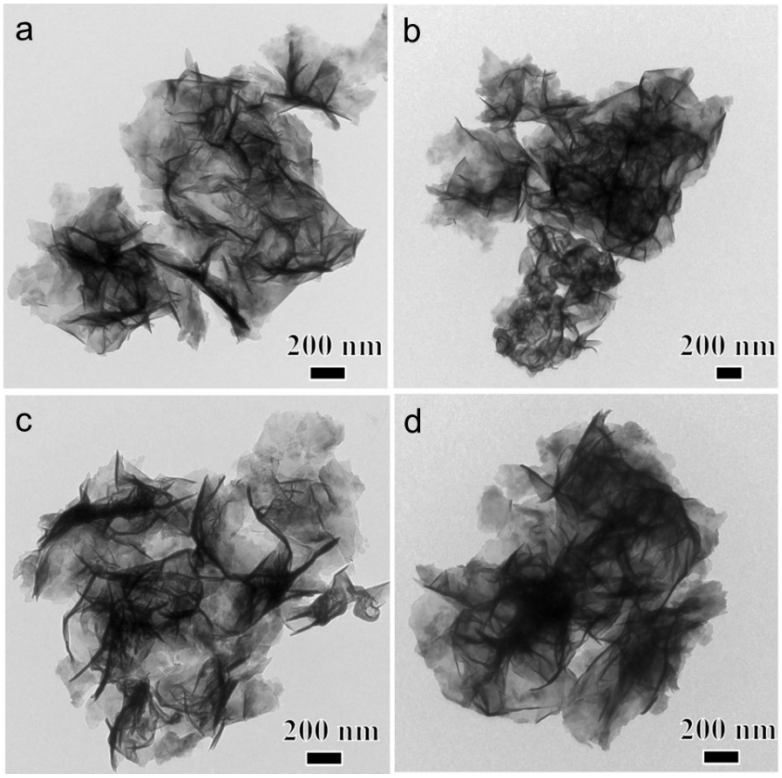

Fig. S12 TEM images of Cu-SnS_2-S_V nanosheets with various Cu doping molar percentages: (a) 1.25%, (b) 2.5%, (c) 5%, and (d) 20%.

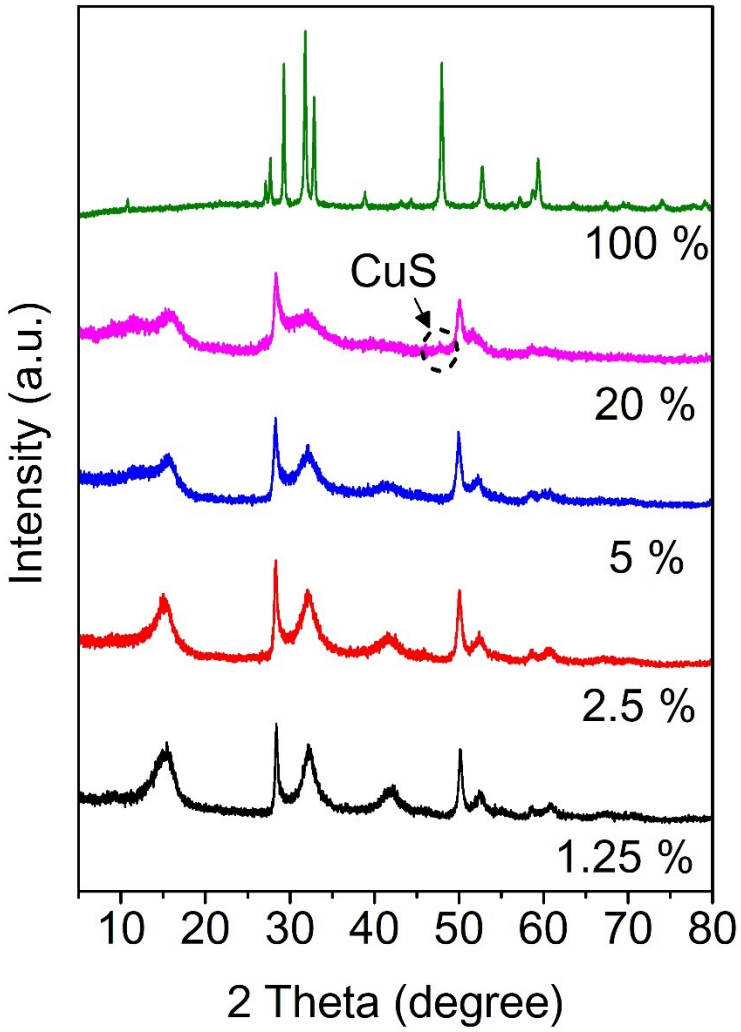

Fig. S13 XRD patterns of the Cu-SnS_2-S_V nanosheets with various Cu doping concentrations. The sample with 100% Cu doping level refers to CuS.

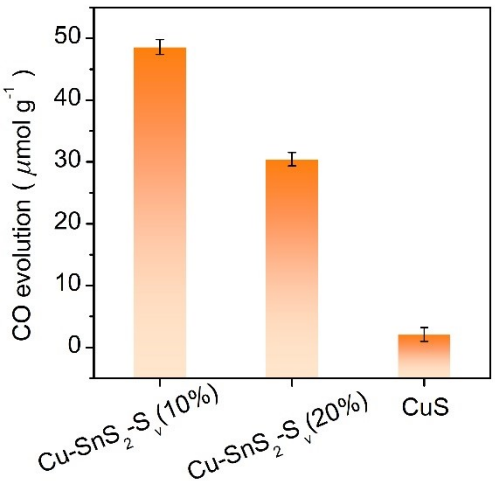

Fig. S14 Photocatalytic CO production over various samples.

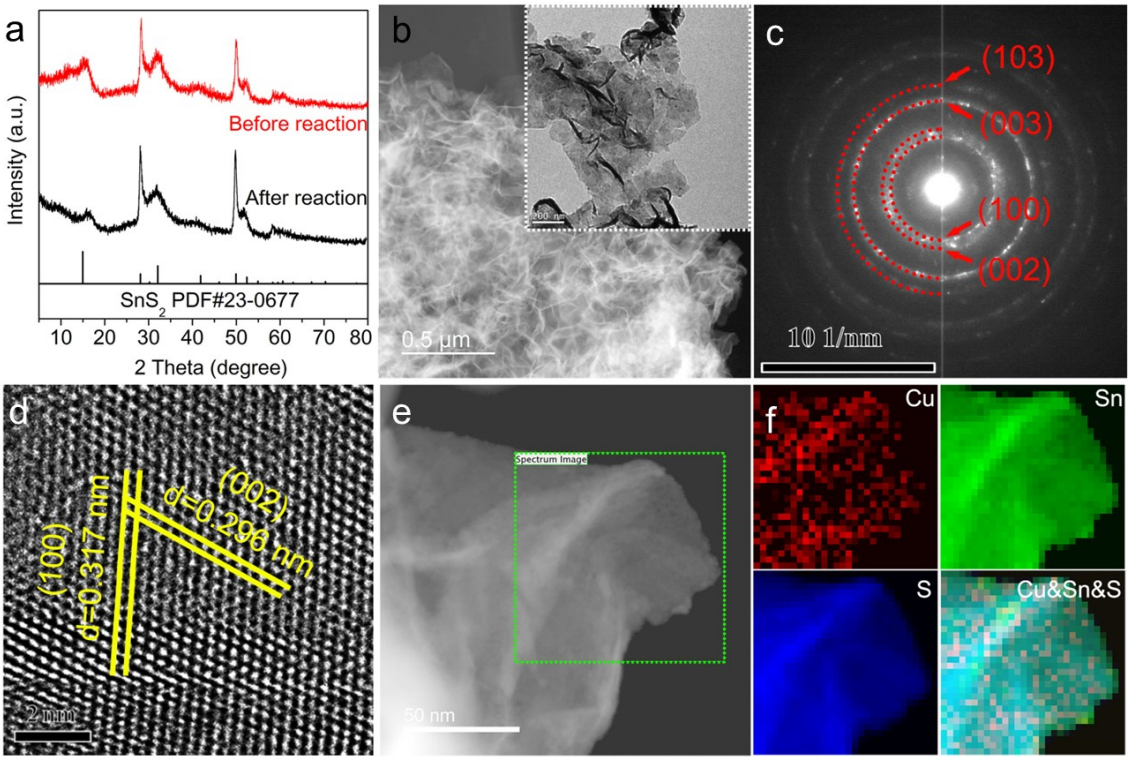

Fig. S15 (a) XRD patterns of the recovered Cu-SnS_2-S_V catalyst and the fresh Cu-SnS_2-S_V catalyst. (b) STEM image (the inset is the TEM image), (c) SAED pattern, (d) HRTEM image, and (e) HAADF-STEM image and (f) its corresponding EELS elemental mapping of the recovered Cu-SnS_2-S_V catalyst.

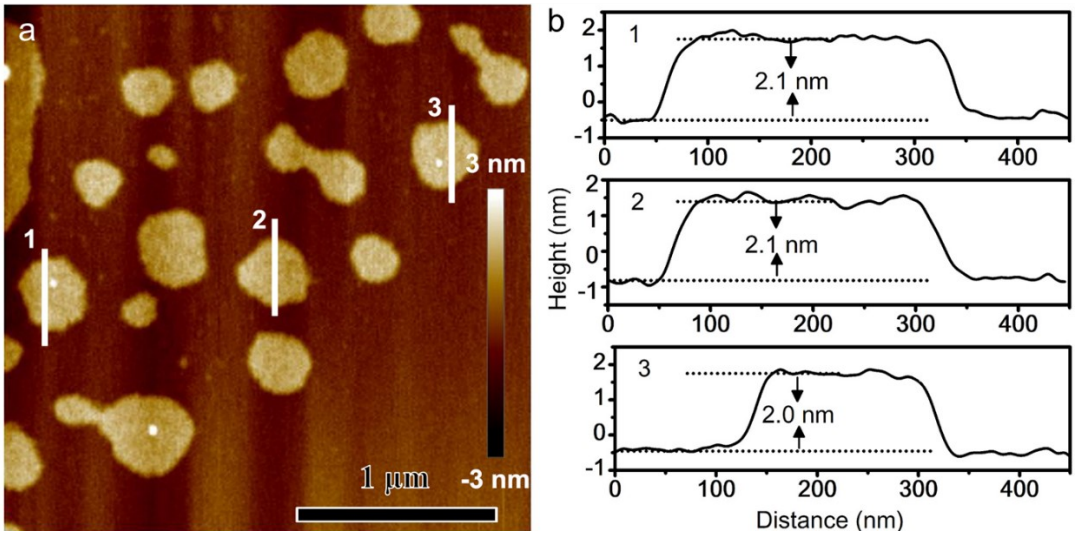

Fig. S16 (a) AFM image of the recovered Cu-SnS_2-S_V catalyst and (b) its corresponding height profile.

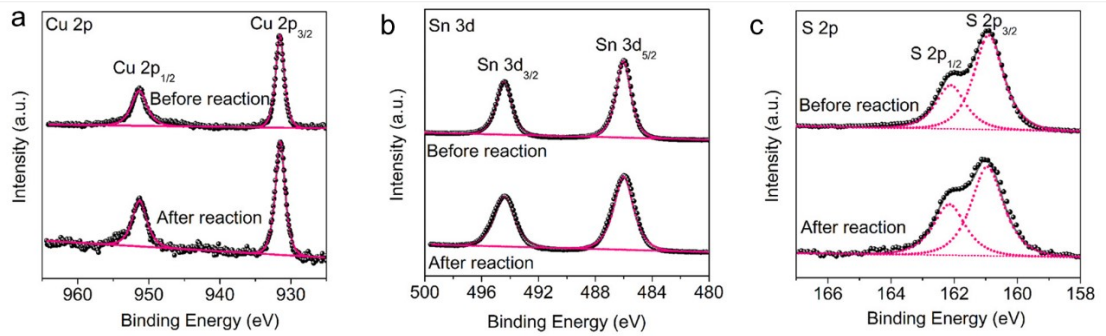

Fig. S17 XPS spectra of the recovered Cu-SnS_2-S_V catalyst: (a) Cu 2p, (b) Sn 3d, and (c) S 2p.

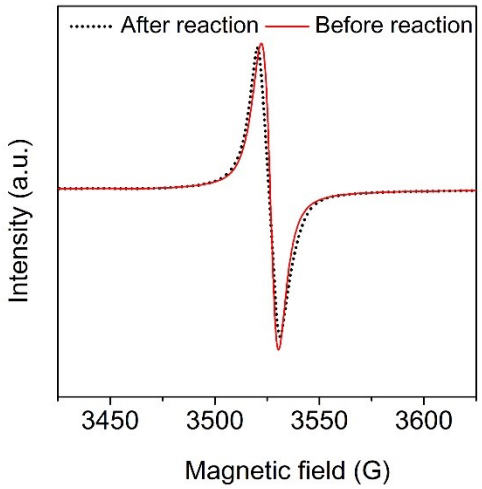

Fig. S18 ESR spectra of Cu-SnS_2-S_V before and after CO_2 reduction.

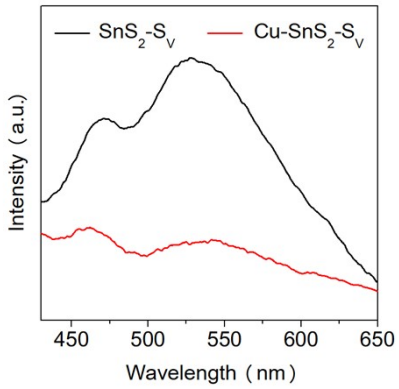

Fig. S19 Steady-state PL spectra of Cu- SnS_2-S_V and SnS_2-S_V.

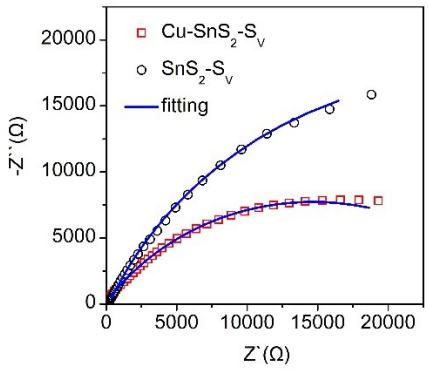

Fig. S20 EIS spectra of Cu-SnS_2-S_V and SnS_2-S_V.

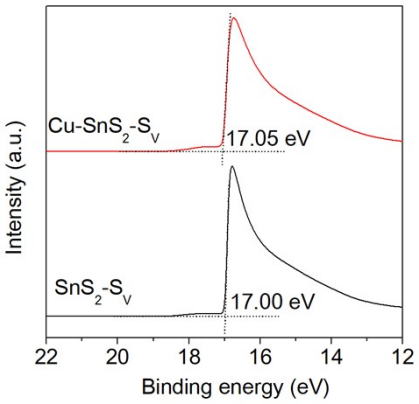

Fig. S21 UPS spectra of Cu-SnS_2-S_V and SnS_2-S_V.

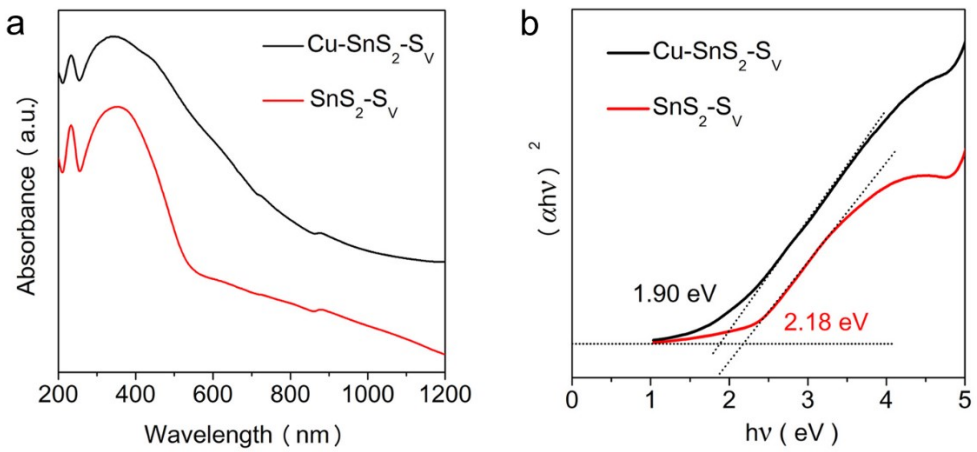

Fig. S22 (a) UV-Vis spectra of Cu-SnS_2-S_V and SnS_2-S_V, and (b) their corresponding Tauc plots.

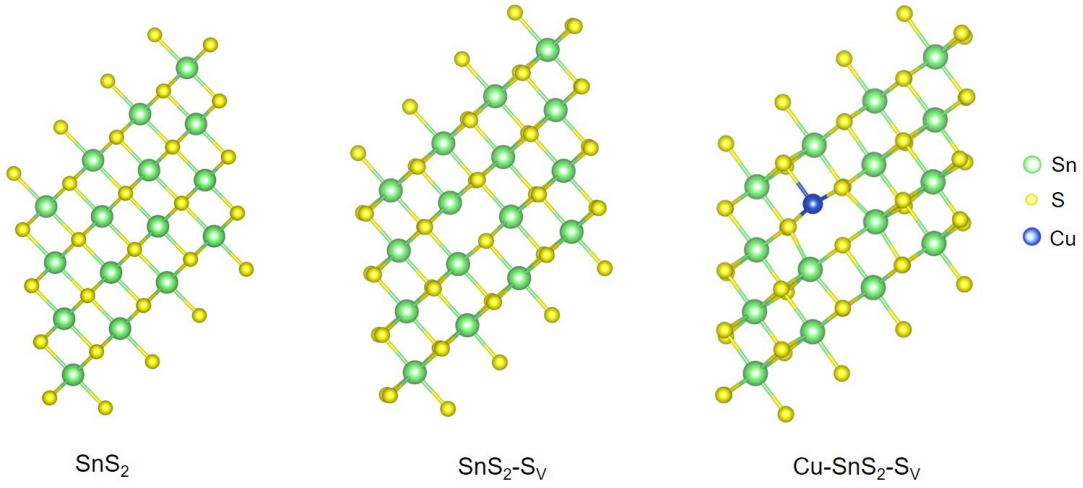

Fig. S23 The optimized structures of the SnS_2, SnS_2-S_V, and Cu-SnS_2-S_V slabs.

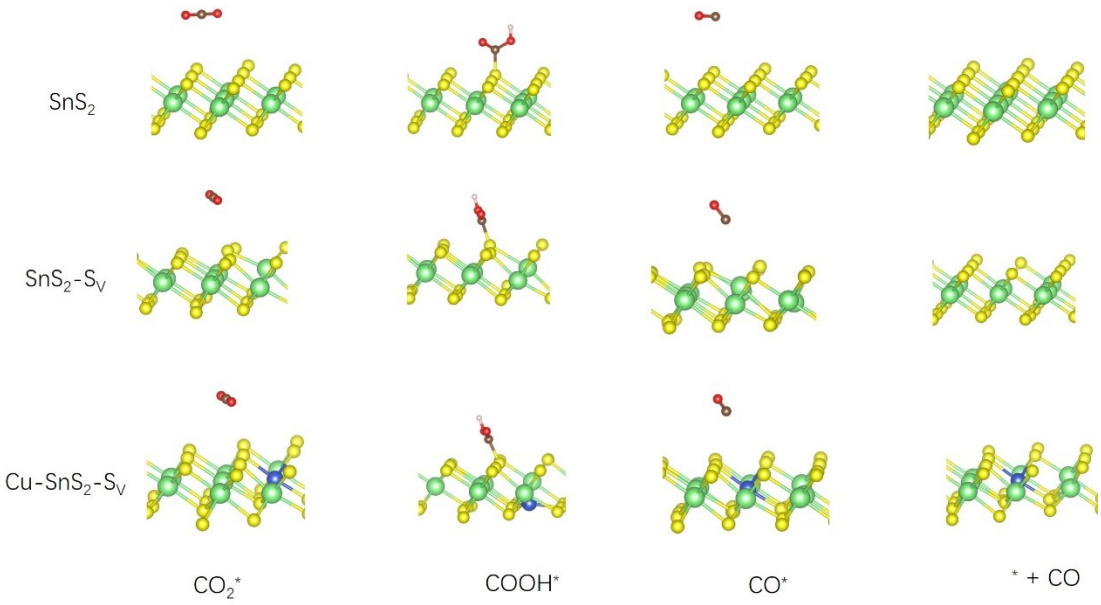

Fig. S24 The optimized geometric structure of reaction intermediates adsorbed on the various substrates.

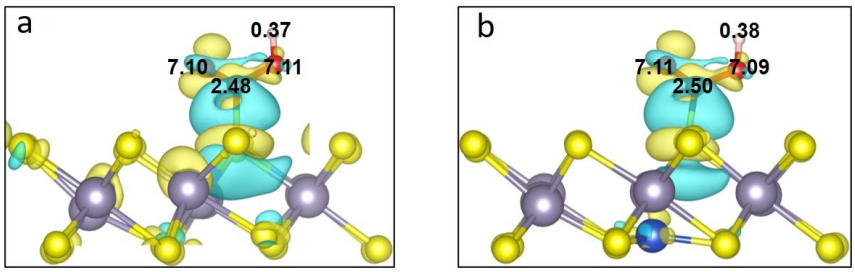

Fig. S25 The calculated Bader of the adsorbed COOH* on SnS_2-S_V (a) and Cu-SnS_2-S_V (b). Iso-surface value is set to be 0.002 e $Bohr^{-3}$, and the charge accumulation and depletion are shown in yellow and cyan, respectively.

Table S1. EXAFS fitting parameters at the Cu K-edge for different samples.

Sample	Shell	C.N.	R (Å)	ΔE_0 (eV)	σ^2(Å^2)	S_0^2	R factor
Cu foil	Cu-Cu	12	2.54(1)	4.1	0.008(3)	0.85	0.2%
CuS	Cu-S	4.1(4)	2.24(7)	0.3	0.011(1)	0.86	0.7%
Cu-SnS_2-S_V	Cu-S	3.2(2)	2.26(5)	2.2	0.007(1)	0.80	0.6%

C.N.: coordination numbers; R: interatomic distance; ΔE_0: edge-energy shift (the difference between the zero kinetic energy value of the sample and that of the theoretical model); σ^2: Debye-Waller factor (a measure of thermal and static disorder in absorber-scatterer distances); S_0^2: amplitude reduction factor; R factor: goodness of the fitting.

Table S2. The CO evolution activity comparison of our work with the previous reports without using electron donors or photosensitizer.

Photocatalysts	CO evolution rate (umol/g/h)	AQY (%)	References
Cu-SnS_2-S_V	48.6	0.34 (420 nm)	This work
Cu_2ZnSnS_4/Pt/g-C_3N_4	17.4	0.41 (533 nm)	[6]
CdSe/$SnNb_2O_6$	36.1	-	[7]
MnO_x/CeO_2@SnS_2/Ni_2P	29.7	0.76 (420 nm)	[8]
$SnFe_2O_4$-g-C_3N_4	7.6	-	[9]
Cu_3SnS_4	8.48	-	[10]
In_4SnS_8	~20.1	0.13 (475 nm)	[11]
SnS_2/SnO_2	12.3	-	[12]
SnS_2	12.7	-	[13]
S_v-Cu_3SnS_4	18.4	0.66 (420 nm)	[14]
SnS_2/TiO_2	58.0	-	[15]
SnS_2/SnO_2	48.0	0.015 (420 nm)	[16]
SnS_2/g-C_3N_4/C	40.9	-	[17]
WO_3-TiO_2/Cu_2ZnSnS_4	15.4	0.36 (420 nm)	[18]
$SnTa_2O_6$	28.0	-	[19]
V_S-SnS_2	25.7	0.028 (420 nm)	[20]

Table S3. The fitted photoluminescence lifetime values by using a bi-exponential function fitting curves.

Samples	A_1 (%)	τ_1 (ns)	A_2 (%)	τ_2 (ns)	$\tau_{Average}$ (ns)
SnS_2-S_V	99.79	0.06	0.21	11.26	3.23
Cu- SnS_2-S_V	99.35	0.08	0.65	13.05	6.78

SI References

1. G. Kresse and J. Furthmüller, *Phys. Rev. B*, 1996, **54**, 11169.
2. G. Kresse and D. Joubert, *Phys. Rev. B*, 1999, **59**, 1758.
3. P. E. Blöchl, *Phys. Rev. B*, 1994, **50**, 17953.
4. J. P. Perdew, K. Burke and M. Ernzerhof, *Physical review letters*, 1996, **77**, 3865.
5. M. He, Y. Wu, R. Li, Y. Wang, C. Liu and B. Zhang, *Nat. Commun.*, 2023, **14**, 5088.
6. A. Raza, H. Shen and A. A. Haidry, *Appl. Catal. B*, 2020, **277**, 119239.
7. X. Ke, J. Zhang, K. Dai, K. Fan and C. Liang, *Sol. RRL*, 2021, **5**, 2000805.
8. Z. Guan, Y. Chen, Y. Ding, J. Lin, Y. Zhao, Y. Jiao and G. Tian, *Appl. Surf. Sci.*, 2022, **592**, 153192.
9. Y. Jia, H. Ma, W. Zhang, G. Zhu, W. Yang, N. Son, M. Kang and C. Liu, *Chem. Eng. J.*, 2020, **383**, 123172.
10. N. Sharma, T. Das, S. Kumar, R. Bhosale, M. Kabir and S. Ogale, *ACS Appl. Energy Mater.*, 2019, **2**, 5677-5685.
11. Y. Chai, Y. Chen, J. Shen, M. Ni, B. Wang, D. Li, Z. Zhang and X. Wang, *ACS Catal.* 2021, **11**, 11029-11039.
12. X. Jiao, X. Li, X. Jin, Y. Sun, J. Xu, L. Liang, H. Ju, J. Zhu, Y. Pan, W. Yan, Y. Lin and Y. Xie, *J. Am. Chem. Soc.*, 2017, **139**, 18044-18051.
13. F. You, X. Hou, P. Wei and J. Qi, *Inorg. Chem.*, 2021, **60**, 18598-18602.
14. J. Wang, T. Bo, B. Shao, Y. Zhang, L. Jia, X. Tan, W. Zhou and T. Yu, *Appl. Catal. B*, 2021, **297**, 120498.
15. A. Han, M. Li, S. Zhang, X. Zhu, J. Han, Q. Ge and H. Wang, *Catal.*, 2019, **9**, 927.
16. F. You, J. Wan, J. Qi, D. Mao, N. Yang, Q. Zhang, L. Gu and D. Wang, *Angew. Chem. Int. Ed.,* 2020, **59**, 721-724.
17. Y. Li, Q. Yin, Y. Zeng and Z. Liu, *Chem. Eng. J.*, 2022, **438**, 135652.
18. A. Raza, H. Shen, A. A. Haidry, L. Sun, R. Liu and S. Cui, *J. CO_2 Util.*, 2020, **37**, 260-271.
19. J. Zhao, Z. Xiong, J. Wang, Y. Qiu, P. Liu, Y. Zhao and J. Zhang, *Chem. Eng. J.*, 2022, **446**, 137242.
20. S. Yin, X. Zhao, E. Jiang, Y. Yan, P. Zhou and P. Huo, *Energy Environ. Sci.*, 2022, **15**, 1556-1562.